DRAFT VERSION NOVEMBER 8, 1999
Preprint typeset using LaTeX style emulateapj

RELATIVISTIC JETS FROM COLLAPSARS

M.A. ALOY[1], E. MÜLLER[2], J.M$^{\underline{\mathrm{A}}}$ IBÁÑEZ[1], J.M$^{\underline{\mathrm{A}}}$ MARTÍ[1] AND A. MACFADYEN[3]

Draft version November 8, 1999

ABSTRACT

We have studied the relativistic beamed outflow proposed to occur in the collapsar model of gamma-ray bursts. Using a collapsar progenitor model of MacFadyen & Woosley we have simulated the propagation of an axisymmetric jet through a collapsing rotating massive star with the GENESIS multi-dimensional relativistic hydrodynamic code. The jet forms as a consequence of an assumed constant or variable energy deposition in the range 10^{50} erg s^{-1} to 10^{51} erg s^{-1} within a 30° cone around the rotation axis. The jet flow is strongly beamed ($\lesssim$ few degrees), spatially inhomogeneous, and time dependent. The jet reaches the surface of the stellar progenitor ($R_* = 2.98 \times 10^{10}$ cm) intact. At breakout the maximum Lorentz factor of the jet flow ($\Gamma_{\rm max}$) is 33 for a purely energy driven jet. After breakout the jet accelerates into the circumstellar medium, whose density is assumed to decrease exponentially and then being constant. Outside the star the flow begins to expand also laterally ($v \sim c$), but the beam remains very well collimated. At a distance of $2.54 \times R_*$, where we had to stop the simulation, the Lorentz factor has increased to 44.

Subject headings: gamma-rays: bursts — hydrodynamics — methods: numerical — relativity

1. INTRODUCTION

Various catastrophic collapse events have been proposed to explain the energies released in a gamma-ray burst (GRB) including mergers of compact binaries (Pacyński 1986; Goodman 1986; Eichler *et al.* 1989; Mochkovitch *et al.* 1993), collapsars (Woosley 1993) and hypernovae (Pacyński 1998). According to the current view these models require a common engine, namely a stellar mass black hole (BH) which accretes up to several solar masses of matter. A fraction of the gravitational binding energy released by accretion is thought to power a pair fireball. If the baryon load of the fireball is not too large, the baryons are accelerated together with the e^+e^- pairs to Lorentz factors $> 10^2$ (Cavallo & Rees 1978). Such relativistic flows are supported by radio observations of GRB 980425 (Kulkarni *et al.* 1998b).

Spherically symmetric fireballs have been studied by several authors by means of 1D Lagrangian hydrodynamic simulations (*e.g.*, Panaitescu *et al.* 1997; Panaitescu & Mészáros 1998; Kobayashi, Piran & Sari 1999). Recently, it has been argued that the rapid temporal decay of several GRB afterglows is more consistent with the evolution of a relativistic jet after it slows down and spreads laterally than with a spherical blast wave (Sari, Piran & Halpern 1999; Halpern *et al.* 1999; Kulkarni *et al.* 1999; Rhoads 1999). The lack of a radio afterglow in GRB 990123 provides independent evidence for jet-like geometry (Kulkarni *et al.* 1999b). Motivated by these observations and by the collapsar model of MacFadyen & Woosley (1999; henceforth MW99) we have simulated the propagation of jets from collapsars using relativistic hydrodynamics.

2. INITIAL MODEL AND NUMERICAL SETUP

MW99 have explored the evolution of rotating helium stars ($M_\alpha \gtrsim 10 M_\odot$) whose iron core collapse does not produce a successful outgoing shock, but instead forms a BH surrounded by a compact accretion torus. Assuming that the efficiency of energy deposition is higher in the polar regions MW99 obtain relativistic jets along the rotation axis, which remain highly focused and seem capable of penetrating the star. However, as their simulations were performed with a Newtonian code, they obtain speeds in the jet flow which are appreciably superluminal.

We have performed axisymmetric relativistic simulations using a $14 M_\odot$ collapsar model from MW99. When the central BH has acquired a mass of $3.762 M_\odot$ we map the model to our computational grid. In a consistent collapsar model a jet will be launched by any process which gives rise to a local deposition of energy and/or momentum, as *e.g.*, $\nu\bar{\nu}$–annihilation, or magnetohydrodynamic processes. We mimic such a process by depositing energy at a prescribed rate homogeneously within a 30° cone around the rotation axis. In the radial direction the deposition region extends from the inner grid boundary located at 200 km to a radius of 600 km. We have investigated two constant energy deposition rates $\dot{E} = 10^{50}$ erg s^{-1} and $\dot{E} = 10^{51}$ erg s^{-1}, and a varying deposition rate with a mean value of 10^{50} erg s^{-1}. The constant rates roughly bracket the expected $\dot{E}$ of collapsar models, while the varying rate mimics, *e.g.*, time-dependent mass accretion rates resulting in time-dependent $\nu\bar{\nu}$–annihilation (MW99).

The simulations were performed with the multidimensional relativistic hydrodynamic code GENESIS (Aloy *et al.* 1999) using 2D spherical coordinates (r, θ). In the r–direction the computational grid consists of 200 zones spaced logarithmically between the inner boundary and the surface of the helium star at $R_* = 2.98 \times 10^{10}$ cm. Assuming equatorial symmetry we performed simulations with $2°, 1°$ and $0.5°$ angular resolution. In the latter case the grid consists of 60 uniform zones covering the polar region ($0° \le \theta \le 30°$) and 40 nonuniform zones logarithmically distributed between $30° \le \theta \le 90°$.

The gravitational field is described assuming a Schwarzschild BH space–time. Effects due to the self-gravity of the star on the dynamics are neglected. The equation of state includes the contributions of non-relativistic nucleons treated as a mixture of Boltzmann gases, radiation, and an approximate correction due to e^+e^-–pairs as described in Witti, Janka & Takahashi (1994).

[1]Departamento de Astronomía y Astrofísica, Universidad de Valencia, 46100 Burjassot (Valencia), Spain
[2]Max-Planck-Institut für Astrophysik, Karl-Schwarzschild-Str. 1, 85748 Garching, Germany
[3]Astronomy Department, University of California, Santa Cruz, CA 95064

Complete ionization is assumed, and the effects due to degeneracy are neglected. We advect nine non-reacting nuclear species which are present in the initial model: C^{12}, O^{16}, Ne^{20}, Mg^{24}, Si^{28}, Ni^{56}, He^4, neutrons and protons.

3. RESULTS

3.1. *Constant small energy deposition rate (Model C50)*

For a constant $\dot{E} = 10^{50}\,\mathrm{erg\,s^{-1}}$ a relativistic jet forms within a fraction of a second and starts to propagate along the rotation axis with a mean speed of $7.8\times10^9\,\mathrm{cm\,s^{-1}}$ (Fig. 1). The jet exhibits all the morphological elements of the Blandford & Rees (1974) jet model: a terminal bow shock, a narrow cocoon, a contact discontinuity separating stellar and jet matter, and a hot spot. Fig. 1 shows that the density structure of the star does not change noticeably during the whole evolution. This, a posteriori, justifies our neglect of the self-gravity of the star.

The propagation of the jet is unsteady, because of density inhomogeneities in the star. The Lorentz factor of the jet, Γ, increases non-monotonically with time, while the density drops to $\sim 10^{-6}\,\mathrm{g\,cm^{-3}}$ (Fig. 2). The density profile shows large variations (up to a factor of 100) due to internal shock waves. The mean density in the jet lies in the range $10^{-2} - 1\,\mathrm{g\,cm^{-3}}$. Some of the internal biconical shocks, which develop during the jet's propagation, recollimate the beam. They may provide the "internal shocks" proposed to explain the observed gamma-ray emission. A particularly strong recollimation shock wave (hardly evident at low resolution) forms early in the evolution. A very strong rarefaction wave behind this recollimation shock causes the largest local acceleration of the beam material giving rise to a maximum in the Lorentz factor. When the jet encounters a region along the axis where the density gradient is positive (at $\log r \approx 8.1$ and $\log r \approx 8.6$) the jet's head is decelerated, while a central channel in the beam is cleaned by outflow into the cocoon through the head, which accelerates the beam. The combination of both effects (deceleration of the head and beam acceleration) increases the strength of the internal shocks.

Within the jet the mean value of the specific internal energy, $\sim 10^{20} - 10^{21}\,\mathrm{erg\,g^{-1}}$, or $\sim O(c^2)$. The mean temperature $\sim 5\times10^8$ K (well below the pair creation threshold) is independent of resolution implying that the pressure is radiation dominated in accordance with our simplified EOS.

The relativistic treatment of the hydrodynamics leads to a qualitatively similar (formation of a jet), but quantitatively very different evolution than in MW99. Some quantitative difference is expected due to the different mapping time and inner boundary radius in the two calculations. According to their Fig. 27 the jet propagates 7,000 km within the first 0.824 s. Furthermore, MW99 infer an asymptotic Lorentz factor ~ 10, and find a half opening angle for their jet of $\sim 10^\circ$. In our simulation, at the same time for the same angular resolution ($\sim 2^\circ$) and $\dot{E}$ the head reaches a radius of 30 000 km, but the maximum Lorentz factor (Γ_{max}) is only 4.62 (at $r \approx 12{,}200$ km). Such quantitative difference is expected, in part, due to different mapping time and inner boundary radius between the two calculations. Initially, in our simulations the half opening angle is between 6° to 8° dependent on angular resolution. At ~ 1.5s the strong recollimation shock reduces the half opening angle to less than 1°. This effect is most remarkable in those models having the best resolution.

We find that some results are strongly depending on angular resolution, the minimum acceptable one being 0.5° (at least near the axis). The morphology of the jet is richer at higher resolution. At 0.5° angular resolution $\Gamma_{\mathrm{max}} \approx 15-20$ (at jet breakout) at a radius $\sim 8\times10^9$ cm. Within the uncertainties of the jet mass determination due to finite zoning and the lack of a precise numerical criterion to identify jet matter, the baryon load ($\eta \equiv Mc^2/E_{\mathrm{depos}}$) seems to decrease with increasing resolution. In the highest resolution run we find an average baryon load of $\eta \simeq 1.3$ at jet breakout (see also Section 4).

3.2. *Constant large energy deposition rate (Model C51)*

Enhancing $\dot{E}$ by a factor of ten (to $10^{51}\,\mathrm{erg\,s^{-1}}$), the jet flow reaches larger Lorentz factors. We observe transients during which the Lorentz factor becomes as large as 40. After 1.2 s the Lorentz factor steadily increases from 22 to 33. The jet propagates faster than in model C50. The time required to reach the surface of the star is 2.27 s instead of 3.35 s. The opening angle of the jet at breakout is $\sim 10^\circ$, *i.e.,* the jet is less collimated. The strong recollimation shock present in model C50 is not so evident here. Instead, several biconical shocks are observed within a very knotty beam and the Lorentz factor near the head of the jet is larger (~ 22 in the final model) because, due to the larger $\dot{E}$, the central funnel is evacuated faster, and because the mean density of the jet is 5 times smaller than in model C50 (η being twice as large).

3.3. *Varying energy deposition rate (Model V50)*

We have computed a model where the mean energy deposition rate ($10^{50}\,\mathrm{erg\,s^{-1}}$) randomly varies on time scales of a few milliseconds and the amplitude by a factor of ten. Compared to model C50 the jet structure is more knotty and also richer in shocks, particularly inside the first 10^9 cm (where the radial resolution is sufficiently large to capture the finest structures imprinted on the flow by the time variability of the deposition rate). At breakout $\Gamma_{\mathrm{max}} = 26.81$, which is *almost twice* as large as the one found in model C50. Thus, a variable $\dot{E}$ is more efficient in converting internal energy into kinetic energy, because the internal shocks are stronger and more numerous in model V50. The mean propagation speed is similar in both models, although the instantaneous velocity of the jet's head is clearly different. The opening angle behind the strongest recollimation shock is quite small ($< 1^\circ$) in both models.

3.4. *Evolution after jet breakout*

The structure of the external medium surrounding the progenitor will influence the characteristics of the GRB and of the subsequent afterglow. Thus, a continuation of the simulations beyond jet breakout is necessary. In order to satisfy the conditions for accelerating shocks (Shapiro 1979) we endowed the star with a Gaussian atmosphere, which at $R_{\mathrm{a}} = 1.8\,R_*$ passes over into an external uniform medium with a density $10^{-5}\,\mathrm{g\,cm^{-3}}$ and a pressure $10^{-8}p(R_*)$. The computational domain is extended to $R_t = 2.54 R_*$ with 70 additional zones. The evolution after jet breakout has been computed for models C50 and C51. In both cases the jet reaches R_t after ~ 1.8 s (measured from breakout). Its mean propagation velocity is ~ 0.85 c, which is almost three times faster than the velocity of the head inside the star (0.30 c in model C50; 0.44 c in model C51).

The evolution after jet breakout consists of three distinct epochs (Fig. 3). The first one lasting 0.35 s is characterized by a head velocity of 0.48 c and a small sideways expansion. During the second phase (from 3.7 s to 4 s) the jet head accelerates to 0.91 c, because of the steep external density gradient, and because the flux of axial momentum is still important compared to pressure. The sideways expansion is still sub-relativistic ($\approx$

0.008 c), and the half opening angle of the beam increases to $\approx 10°$. >From 4 s to 5.2 s the bow-shock propagates within the uniform part of the ambient medium leading to a rapid lateral spreading (Fig. 3) with a velocity $\lesssim$ c in agreement with the estimate of Sari, Piran & Halpern (1999), but larger than that of Rhoads (1999), who predicts a lateral spreading with the maximum sound speed $c_s = c/\sqrt{3}$.

$\Gamma_{\rm max}$ is again obtained behind the first strong recollimation shock. The Lorentz factor near the boundary of the cavity blown by the jet grows from ~ 1 (at jet breakout) to ~ 3 in both models decreasing with latitude. At the end of the simulation $\Gamma_{\rm max}$ is 29.35 (44.17) for model C50 (C51), which is still smaller than the ones required for the fireball model (Piran 1999). However, we point out that the jet has only reached a radius of 7.5×10^{10} cm at the end of our simulations, which is 10^2 to 10^4 times smaller than the distance at which the fireball becomes optically thin. Determining whether a GRB will eventually be produced requires to compute the further evolution of the jet.

The shape of the expanding bubble is prolate (Figs. 1 and 3) during the whole post-breakout evolution. However, when the jet reaches the uniform part of the circumstellar environment, the shape changes appreciably (the jet widens), because the sideways expansion is faster now. We expect a more isotropic expansion when most of the bubble is inside the uniform medium, and when it is pressure driven (in particular if the energy deposition is switched off).

4. DISCUSSION AND CONCLUSIONS

Our simulations show that energy deposition in the polar regions of a collapsar model gives rise to both the formation and propagation of a relativistic jet through the mantle and envelope of the star, and to a supernova explosion. The jet has a small opening angle ($\sim 8°$) and possesses a highly collimated ($\sim 1°$), ultra-relativistic core in which the Lorentz factor reaches a value of $\Gamma_{\rm max} = 44$ (model C51) at the end of the simulation about 2 s after shock breakout. Due to the very good collimation of the outflow the equivalent isotropic kinetic energy (see MacFadyen, Woosley & Heger 1999) slightly exceeds 10^{54} erg for model C51 (10^{53} erg for model C50) within $2°$ ($5°$) of the rotation axis dropping by a factor of 10 within $17°$ ($10°$). The inner region contains $8 \times 10^{-4} M_\odot$ with $<\Gamma>\sim 4$ (Fig. 1). For a larger $\dot{E}$, the jet and in particular the cocoon are less collimated, because when the jet is driven harder it also expands stronger laterally.

The rest-mass density and the internal energy show strong spatial and temporal variations within the jet giving rise to a very inhomogeneous baryon loading. The average baryon load of the jet is $\bar{\eta} \sim 1$, but some parts of the jet have a baryon load $\sim 10^{-5}$ or even less. After jet breakout $\bar{\eta}$ decreases by a factor 4 in less than 1.8 s. If this trend continues $\bar{\eta} \sim 10^{-3}$ within 9 s.

In model C51, at the end of the simulation, $\sim 2M_\odot$ have a Lorentz factor of less than three, $3 \times 10^{-4} M_\odot$ move with $3 \leq \Gamma < 10$, and for $2 \times 10^{-6} M_\odot$ the Lorentz factor $\Gamma \geq 10$ (Fig. 4). The latter two masses reduce to $2 \times 10^{-5} M_\odot$ and $2 \times 10^{-7} M_\odot$ for model C50. Except for the very early evolution ($t < 1$ s) the amount of matter moving at moderate ($3 \leq \Gamma < 10$) and highly ($\Gamma \geq 10$) relativistic velocities increases by a factor ~ 3 every second, *i.e.*, if the central engine is active for another 5 s at the assumed energy deposition rate, $\sim 10^{-4} M_\odot$ will move with $\Gamma \geq 10$. As the maximum Lorentz factor is also rapidly increasing, it is not unlikely that maximum Lorentz factors of several hundreds can be reached before the central engine is shut off. For models where the released total energy is equal (C50 and V50) the maximum beam Lorentz factor is higher (by a factor of two) for a time-dependent $\dot{E}$.

The propagation of the jet into the circumstellar medium depends on its stratification. Thus, further simulations with different environments are planned. We also want to examine progenitors of different size and internal structure. Larger stars provide longer inertial confinement of the jet probably leading to larger Lorentz factors, if the central engine works at least until the jet reaches the stellar surface. Stars with a less pronounced or no central torus will provide less initial collimation. As our simulations have not been pushed far enough in time yet, they can (at the present stage) neither account for the observational properties of GRBs nor their afterglows. Hence, we plan to extend them to later times and larger radii ($\sim 10^{13}$ cm) using adaptive mesh refinement (AMR) techniques. Finally, we want to move the inner boundary closer to the horizon and substitute the Schwarzschild by a Kerr background metric.

This work has been supported in part by the Spanish DGES (grant PB97-1432) and the CSIC. MAA expresses his gratitude to the Conselleria d'Educació i Ciència de la Generalitat Valenciana for a fellowship. We would like to thank Stan Woosley for his enthusiasm in promoting this work, and Thomas Janka for many helpful remarks. The calculations were performed on two SGI Origin 2000 at the CEPBA and at the SIUV.

REFERENCES

Aloy, M.A., Ibáñez, J.Mª, Martí, J.Mª and Müller, E. (1999), ApJS122, 151
Blandford, R. and Rees, M.J. (1974), MNRAS169, 395
Cavallo, G. and Rees, M.J. (1978), MNRAS183, 359
Eichler, D., Livio, M., Piran, T. and Schramm, D.N., 1989, Nature340, 126
Goodman, J. (1986), ApJ308, L47
Halpern, J.P, Kemp, J., Piran, T. and Bershady, M.A. (1999), ApJ517, L105
Kobayashi, S., Piran, T. and Sari, R. (1999), ApJ513, 669
Kulkarni, S.R., Frail, D.A., Wieringa, M.H., Ekers, R.D., Sadler, E.M., Wark, R.M., Higdon, J.L., Phinney, E.S. and Bloom, J.S. (1998b), Nature395, 663
Kulkarni, S.R., Djorgovski, S.G., Odewahn, S.C., Bloom, J.S., Gal, R.R., *et al.* (1999a), Nature398, 389
Kulkarni, S.R., Frail, D.A., Sari, R., Moriarty-Schieven, G.H., Shepherd, D.S., Udomprasert, P., Readhead, A.C.S., Bloom, J.S., Feroci, M. and Costa, E. (1999b), preprint astro-ph/9903441
MacFadyen, A.I. and Woosley, S.E. (1999), ApJ524, 262 (MW99)
MacFadyen, A.I., Woosley, S.E., and Heger, A. (1999), submitted to ApJ and astro-ph/9910034
Mèszáros, P. (1999), in *Proc. of the 19th Texas Symp. on Relativistic Astrophysics & Cosmology*, Paris, Dec. 1998; and astro-ph/9904038
Mochkovitch, R., Hernanz, M., Isern, J. and Martin, X. (1993), Nature361, 236
Pacyński, B. (1986), ApJ308, L43
Pacyński, B. (1998), ApJ494, L45
Panaitescu, A., Wen, L., Laguna, P. and Mészáros, P. (1997), ApJ482, 942
Panaitescu, A. and Mészáros, P. (1999), ApJ, in press; and astro-ph/9810258
Pian, E., Amati, L., Antonelli, L.A., Butler, R.C., Costa, E., *et al.* (1999), A&A, submitted; and astro-ph/9903113
Piran, T. (1999), Physics Reports, **314**, 575
Rhoads, J.E. (1999), ApJ, submitted; and astro-ph/9903399
Sari, R., Piran, T. and Halpern, J.P. (1999), ApJ519, L17
Shapiro, P.R. (1979), ApJ233, 831
Woosley, S.E. (1993), ApJ405, 273

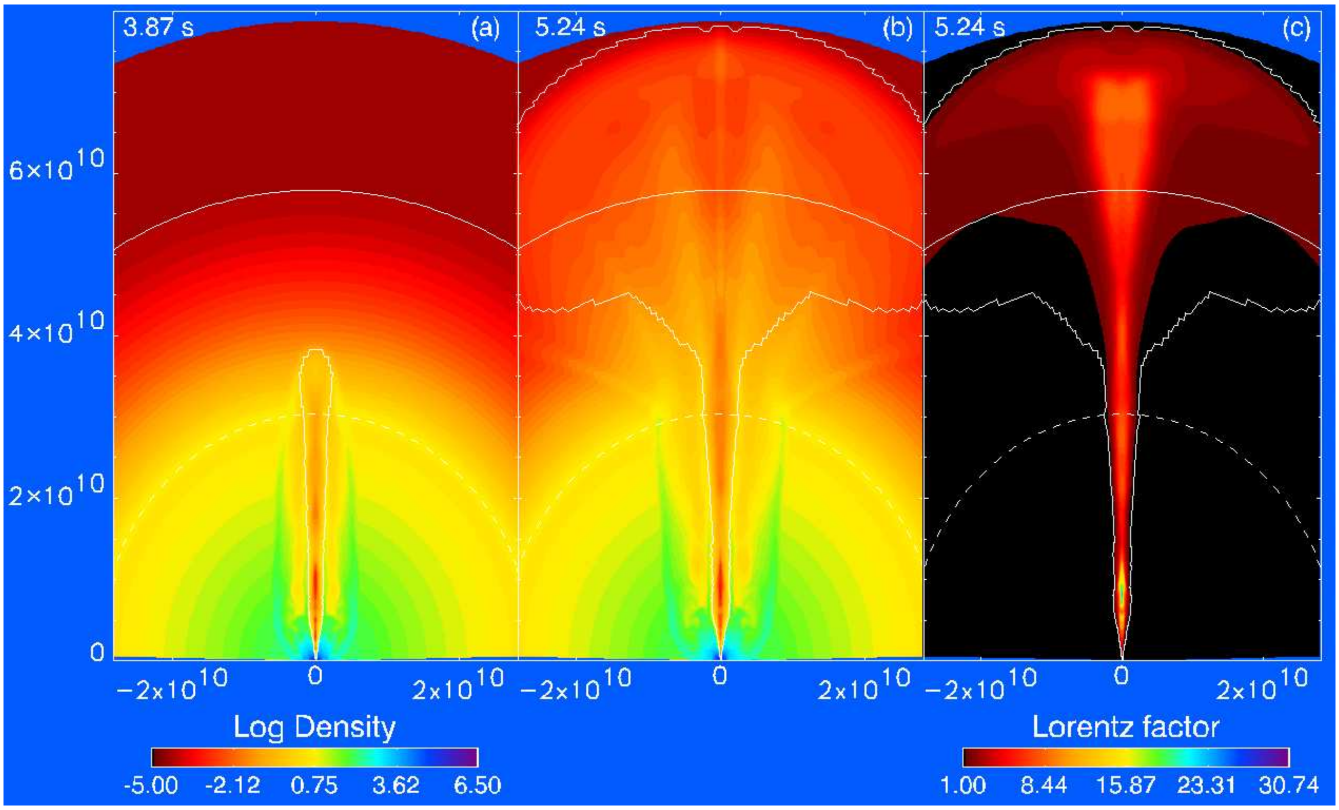

FIG. 1.— Contour maps of the logarithm of the rest–mass density after 3.87 s and 5.24 s (left two panels), and of the Lorentz factor (right panel) after 5.24 s. X and Y axis measure distance in centimeters. The dashed and solid arcs marks the stellar surface and the outer edge of the exponential atmosphere, respectively. The other solid line encloses matter whose velocity is larger than 0.3 c, and whose specific internal energy density is larger than 5×10^{19} erg g^{-1}.

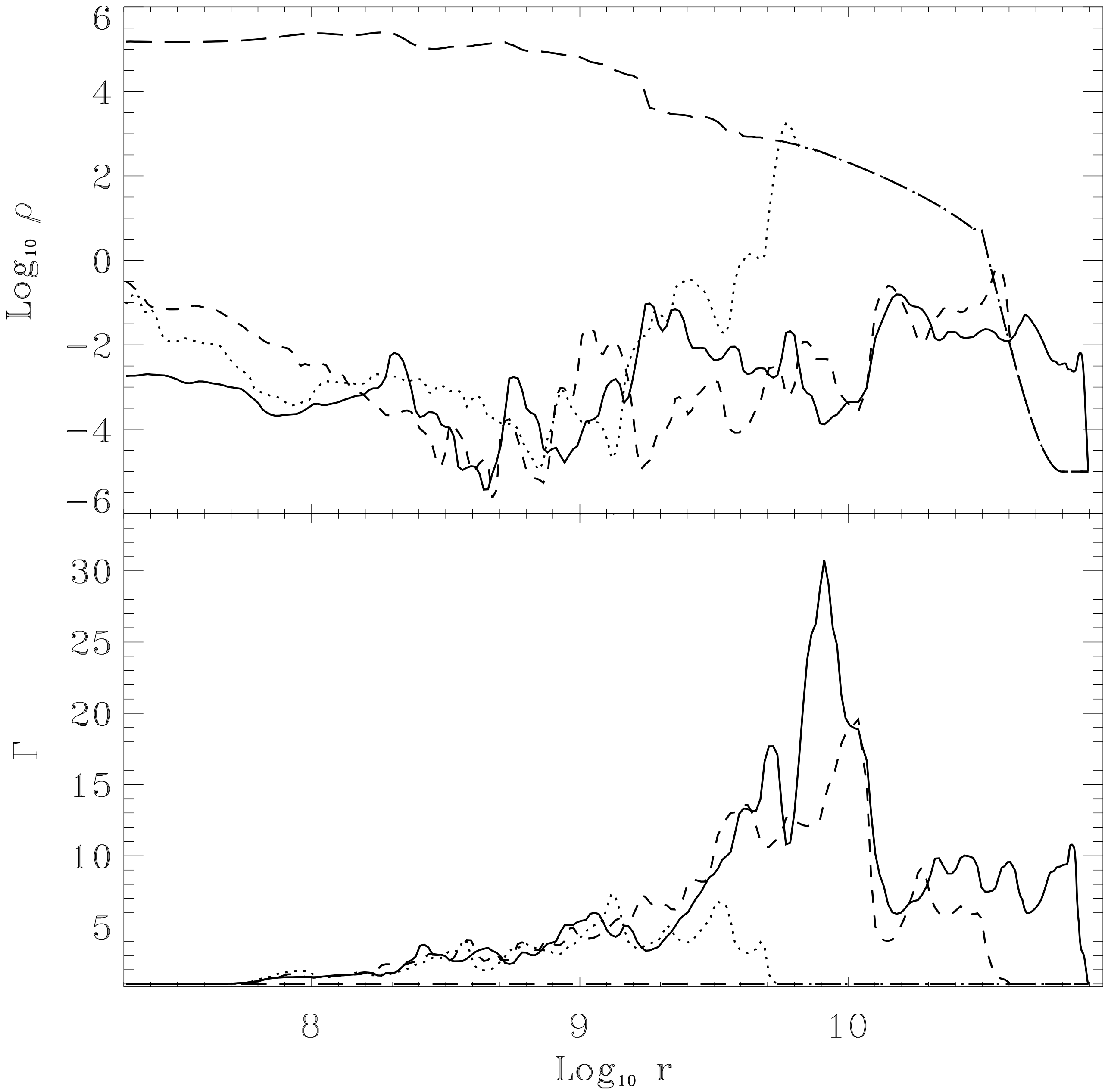

FIG. 2.— Lorentz factor (bottom) and rest–mass density (top) vs radius along the symmetry axis for model C50 at $t = 0$ s (long dashed), $t = 1.44$ s (dotted), $t = 3.87$ s (dashed), and $t = 5.24$ s (solid), respectively.

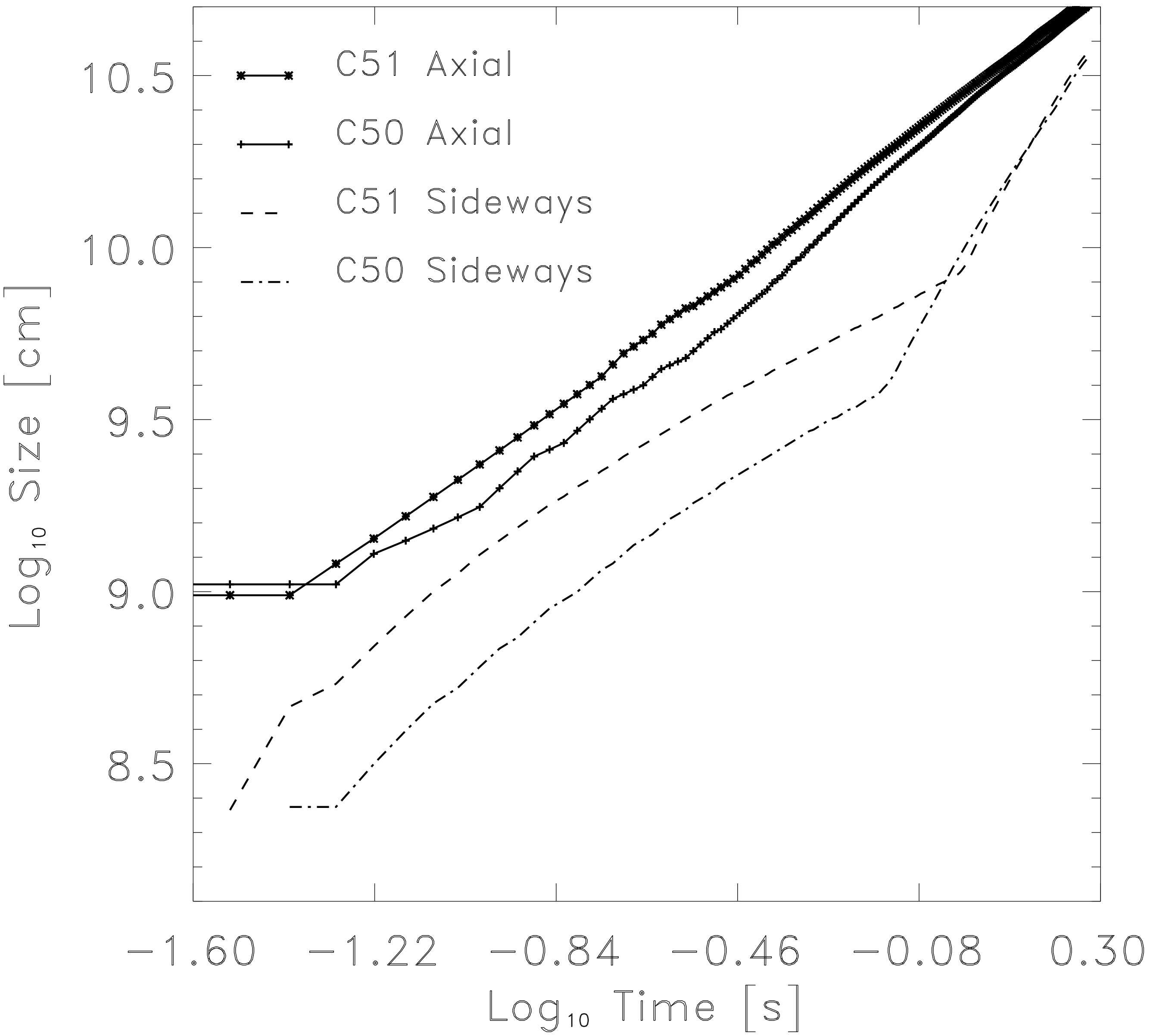

FIG. 3.— Axial and lateral size of the jet driven bubble versus time since jet breakout for models C50 and C51.

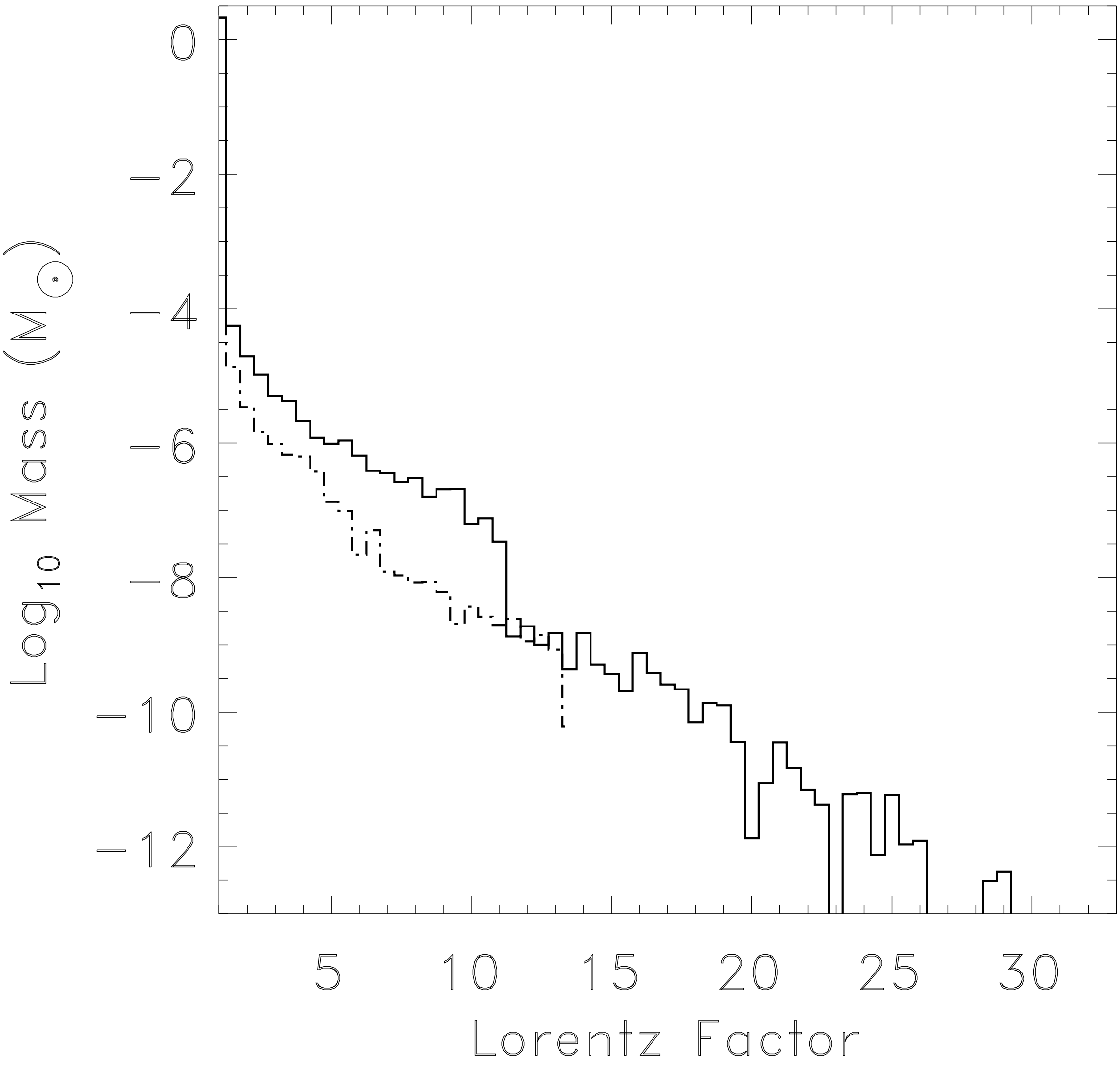

FIG. 4.— Mass (binned in $\Delta\Gamma = 0.5$ intervals) versus Lorentz factor for model C50 at shock breakout (t = 3.87 s; dash-dotted) and at t = 5.24 s (solid), respectively.